

# Geochemistry, Geophysics, Geosystems



## RESEARCH ARTICLE

10.1029/2020GC009246

### Key Points:

- The pre OAE 2 Mo-isotope composition of seawater constrained to 1.1%–1.9%
- Limited change in seawater Mo isotopes during OAE 2 linked to enhanced global Mo burial with Fe minerals
- The response of other redox-sensitive isotopic systems to major ocean redox changes may be affected by global changes in Fe cycling

### Supporting Information:

- Supporting Information S1

### Correspondence to:

A. J. Dickson,  
[alex.dickson@rhul.ac.uk](mailto:alex.dickson@rhul.ac.uk)

### Citation:

Dickson, A. J., Jenkyns, H. C., Idiz, E., Sweere, T. C., Murphy, M. J., van den Boorn, S. H. J. M., et al. (2021). New constraints on global geochemical cycling during Oceanic Anoxic Event 2 (Late Cretaceous) from a 6-million-year long molybdenum-isotope record. *Geochemistry, Geophysics, Geosystems*, 22, e2020GC009246. <https://doi.org/10.1029/2020GC009246>

Received 15 JUN 2020

Accepted 27 OCT 2020

## New Constraints on Global Geochemical Cycling During Oceanic Anoxic Event 2 (Late Cretaceous) From a 6-Million-year Long Molybdenum-Isotope Record

Alexander J. Dickson<sup>1,2</sup> , Hugh C. Jenkyns<sup>1</sup> , Erdem Idiz<sup>1</sup>, Tim C. Sweere<sup>1,3</sup>, Melissa J. Murphy<sup>1</sup>, Sander H. J. M. van den Boorn<sup>4</sup>, Micha Ruhl<sup>1,5</sup>, James S. Eldrett<sup>4</sup>, and Donald Porcelli<sup>1</sup>

<sup>1</sup>Department of Earth Sciences, University of Oxford, Oxford, UK, <sup>2</sup>Department of Earth Sciences, Royal Holloway University of London, Surrey, UK, <sup>3</sup>Department of Earth Sciences, ETH Zürich, Zürich, Switzerland, <sup>4</sup>Shell Global Solutions International B.V., Amsterdam, The Netherlands, <sup>5</sup>Department of Geology, Trinity College Dublin, Dublin 2, Ireland

**Abstract** Intervals of extreme warmth are predicted to drive a decrease in the oxygen content of the oceans. This prediction has been tested for the acme of short (<1 million years) episodes of significant marine anoxia in the Phanerozoic geological record known as Oceanic Anoxic Events (OAEs). However, there is a paucity of data spanning prolonged multimillion-year intervals of geological time before and after OAEs. We present a Mo-isotope record from limestones and marlstones of the Eagle Ford Group, South Texas, which was deposited in the southern Cretaceous Western Interior Seaway of North America during a 6-million-year period encompassing OAE 2 (Late Cenomanian–early Turonian: ~94 Ma). Mo-isotope compositions from deposits that formed in euxinic (sulfidic) conditions before OAE 2 allow the paleo-seawater composition to be constrained to 1.1%–1.9%. This range of values overlaps previous estimates of up to ~1.5% for the peak of OAE 2 determined from similarly sulfidic sediments deposited in the restricted proto-North Atlantic Ocean. Mo-isotopes thus varied by less than a few tenths of per mil across one of the most extreme intervals of global deoxygenation in the Late Phanerozoic. Rather than a limited change in oceanic deoxygenation, we suggest that the new data reflect changes to global iron cycling linked to basalt-seawater interaction, terrestrial weathering and expanded partially oxygenated shallow shelf-seas that played a key role in the burial of isotopically light molybdenum, thus acting as a counterbalance to its removal into sulfidic sediments.

**Plain Language Summary** Ocean deoxygenation is projected to become more pronounced in the future. This environmental change will place stress on marine biota and will alter biogeochemical systems and climate feedbacks. Oceanic Anoxic Events (OAEs) are a rich source of information about marine deoxygenation in the geological past but there are fundamental questions surrounding the true magnitude and pacing of redox change during these events. We demonstrate that the variability in one of the key geochemical tools used to reconstruct past oceanic oxygen declines, molybdenum isotopes, experienced relatively little change across one of the most significant Oceanic Anoxic Events of the Late Phanerozoic. We argue that this limited variability partly reflects geochemical feedbacks that buffered the molybdenum cycle, thereby preventing a major isotope excursion.

## 1. Introduction

The oxygen content of the modern ocean has declined by several percent over the last half century (Weiss, 1970). This decline has been strongly linked with increasing ocean temperatures, which limit the rate of oxygen diffusion into seawater (Schmitko et al., 2017), changing ocean thermal structure (Keeling et al., 2010) and increased biological productivity and organic-matter respiration due to elevated nutrient supply (Watson et al., 2017). Anthropogenic influences, such as enhanced fluxes of iron to marine surface waters, have also been implicated in regional oxygen decline (Ito et al., 2016). However, there is still considerable debate over the quantitative importance of the different forcing mechanisms behind deoxygenation (Shephard et al., 2017). The geological record has much to offer this debate by allowing insights into Earth System controls on dissolved oceanic oxygen content through time.

© 2021. The Authors.

This is an open access article under the terms of the [Creative Commons Attribution-NonCommercial](https://creativecommons.org/licenses/by-nc/4.0/) License, which permits use, distribution and reproduction in any medium, provided the original work is properly cited and is not used for commercial purposes.

The Cretaceous Period was punctuated by several episodes of widespread oceanic deoxygenation called Oceanic Anoxic Events (OAEs) (Jenkyns, 1980, 2010; Schlanger & Jenkyns, 1976). The most significant of these, OAE 2, spans the Cenomanian–Turonian boundary, ~94 Ma (Meyers et al., 2012a). This event, which lasted for a duration of ~500–900 kys (Eldrett et al., 2015a; Gangl et al., 2019; Li et al., 2017; Meyers et al., 2012; Sageman et al., 2006), is characterized by the widespread occurrence of effectively coeval carbonate-lean organic-rich black shales in marine sedimentary deposits (Arthur et al., 1990; Robinson et al., 2017; Schlanger et al., 1987). Estimates of the global expanse of low-oxygen marine conditions for OAE 2 are based on trace-metal concentrations and metal stable-isotope compositions (Clarkson et al., 2018; Dickson et al., 2016; Goldberg et al., 2016; Hetzel et al., 2009; Montoya-Pino et al., 2010; Ostrander et al., 2017; Owens et al., 2016; Sweere et al., 2018; Westermann et al., 2014). These estimates generally span a short period of time before and after OAE 2 and, in the case of molybdenum isotopes, only characterize the extent of seafloor euxinia during the peak of the event itself. Mo-isotope studies have estimated that the seawater Mo-isotope composition at the peak of OAE 2 was ~1.45%. This value has been used to infer that ~2% of the global ocean seafloor was overlain by euxinic water, which is toxic to most forms of marine life (Dickson et al., 2016; Goldberg et al., 2009; Westermann et al., 2014). However, the size of a Mo-isotope shift at the onset of OAE 2– and therefore the amount by which euxinia in the oceans may have expanded compared to the Cenomanian background conditions– is not known. This uncertainty arises because records able to constrain the Mo-isotope composition of pre-OAE 2 seawater are not widely available. The true magnitude of change in the Mo-isotope system in response to one of the most profound episodes of oceanic deoxygenation of the past 150 million years is therefore unknown.

In this study, we use the Mo-isotope composition of organic-rich marlstones and limestones from the Eagle Ford Group of South Texas, USA, to place constraints on the seawater isotopic composition of Late Cretaceous seawater before and after OAE 2. We address two questions: (i) How large was any putative shift in the Mo-isotope composition of Cretaceous seawater across OAE 2? and (ii) How does any such shift relate to the global expansion of marine euxinia that occurred during OAE 2?

## 2. Molybdenum in the Marine Environment

The isotopic composition of Mo in modern seawater ( $\delta^{98/95}\text{Mo}$  of 2.34‰) is globally homogenous and records the balance between molybdenum fluxes to and from the oceans (Nägler et al., 2011; Nakagawa et al., 2012; Siebert et al., 2003). The element has a modern oceanic residence time of ~440 kyrs (Miller et al., 2011). The isotopic composition of Mo added to the oceans has been estimated as ~0.55‰ and is assumed to remain constant over long timescales (King & Pett-Ridge, 2018; Neely et al., 2018), whereas the amount and composition of Mo buried in marine sediments probably fluctuated over geological time, driving changes in seawater isotopic compositions (Chen et al., 2015; Dickson, 2017; Kendall et al., 2017 and references therein). The critical removal fluxes of Mo from the ocean are redox-dependent. Mo adsorbed to manganese oxyhydroxides has an isotopic composition ~3‰ lower than seawater in well-oxygenated depositional settings (Barling & Anbar, 2004; Siebert et al., 2003). Mo adsorbed to iron oxyhydroxides has an isotopic composition ~0.8%–2.2% lower than seawater in oxic to anoxic settings (Goldberg et al., 2009; Scholz et al., 2017). Thiolyated sulfides and/or polymolybdate species have isotopic compositions 0.5%–0.9% lower than seawater and can form in sulfidic conditions above (euxinic) or below the sediment–water interface in association with organic and/or Fe–Mo–S compounds (Dahl et al., 2017; Helz et al., 1996, 2011; Hutchings et al., 2020; Nägler et al., 2011; Neubert et al., 2008; Vorlicek et al., 2019). Enhanced organic-matter burial in the oceans and an associated increase in the removal flux of Mo into sulfidic sediments at the expense of burial into oxic sinks should therefore result in a secular decrease in both the concentration and isotopic composition of molybdenum in seawater (Kendall et al., 2017).

## 3. Stratigraphy of the Iona-1 and Innes-1 Cores

This study uses two research cores, Iona-1 and Innes-1, drilled on the margin of the Maverick Basin that was located on the Comanche Shelf at the Southern end of the Cretaceous Western Interior Seaway (KWIS) (Figure 1). Both cores sample the Eagle Ford Group. Detailed chemostratigraphy, biostratigraphy and

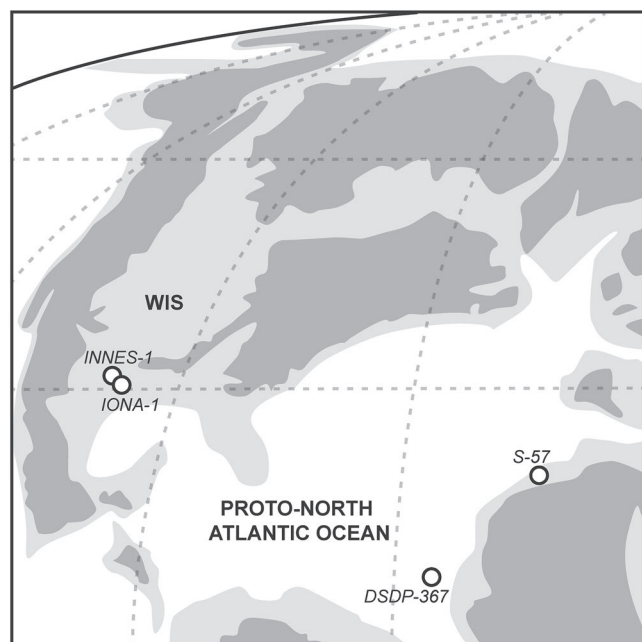


**Figure 1.** Paleogeography of the Cretaceous Western Interior Seaway (WIS) and the proto-North Atlantic Ocean. Locations mentioned in the text are labeled.

sedimentology has previously been undertaken for the two cores (Eldrett et al., 2014, 2015b, 2017; Minisini et al., 2017; Sullivan et al., 2020; Sweere et al., 2020; Figure 2). The Eagle Ford succession is characterized by organic-rich marlstones with decimeter-scale limestone interbeds in the lower Eagle Ford (LEF), and more organic-lean limestones interrupted by decimeter-scale marlstones in the upper Eagle Ford (UEF) (Boling & Dworkin, 2015; Eldrett et al., 2014; Lowery et al., 2014). The onset level of OAE 2, as defined by carbon-isotope stratigraphy, occurs in the uppermost LEF (Eldrett et al., 2014). The LEF is entirely Cenomanian in age, while the UEF is Cenomanian in age at its base (within OAE 2) and Turoonian at the top (post- OAE 2). The major phase of organic-matter deposition and local oxygen depletion in the Eagle Ford Group occurred across a two and half million-year interval prior to the global enhancement of organic-matter burial that took place at many locations during OAE 2 (Boling & Dworkin, 2015; Eldrett et al., 2014; Lowery et al., 2014; Robinson et al., 2017; Schlanger et al., 1987). Similar differences between the timing of local organic-matter accumulation and OAE 2 have been noted from further north in the KWIS, at the transition from the Hartland Shale to the Bridge Creek limestone in Colorado (Arthur and Sageman, 1994).

Local watermasses overlying the Maverick Basin were connected to the proto-North Atlantic Ocean to the south and to the Arctic boreal ocean to the north via the Cretaceous Western Interior Seaway (Eldrett et al., 2017). The occurrence of small-scale cross bedding at the base of the Eagle Ford succession implies the influence of bottom-water currents. Water depths can thus be imprecisely estimated at a few 10s–100s of meters (Eldrett et al., 2017; Minisini et al., 2017).

#### 4. Methods

Core samples were obtained as rock chips and crushed in an agate pestle and mortar. For Mo-isotope and concentration measurements, sample powders were digested in inverse aqua-regia (3:1 HNO<sub>3</sub>-HCl) after the addition of a <sup>100</sup>Mo–<sup>97</sup>Mo double spike to correct for mass fractionation during chemical preparation and mass spectrometry. Following digestion, Mo was purified from matrix elements using the anion-exchange method of Pearce et al. (2010) as modified by Dickson et al. (2016) to remove Zn prior to Mo elution. Measurements were made using 80 ppb (sample plus spike) solutions at the University of Oxford using a Nu-Instruments Nu I MC-ICP-MS coupled to a desolvating sample introduction system. Isotope ratios were calculated offline using the raw measured signal voltages and are expressed in per mil notation relative to NIST 3134, where NIST 3134 has a value of +0.25‰ (Nägler et al., 2014):

$$\delta^{98/95}\text{Mo} = \left( \left( \frac{{}^{98}\text{Mo}}{{}^{95}\text{Mo}}_{\text{sample}} / \frac{{}^{98}\text{Mo}}{{}^{95}\text{Mo}}_{\text{NIST3134}} \right) - 1 \right) * 1000$$

The accuracy and 2 S.D. reproducibility of the method was determined by 33 dissolutions and measurements of the SDO-1 shale standard, giving a value of 1.04% ± 0.08%. This value is in very good agreement with published values (e.g., Goldberg et al., 2013). Mo concentrations were calculated by isotope dilution using the <sup>100</sup>Mo/<sup>95</sup>Mo ratio. Elemental enrichment factors (EF) are calculated according to:

$$\text{EF}_x = \left( \frac{X}{\text{AI}} \right)_{\text{sample}} / \left( \frac{X}{\text{AI}} \right)_{\text{UCC}}$$

Where X is the element being normalized and UCC is the average upper continental crust concentration from Rudnick and Gao (2003).

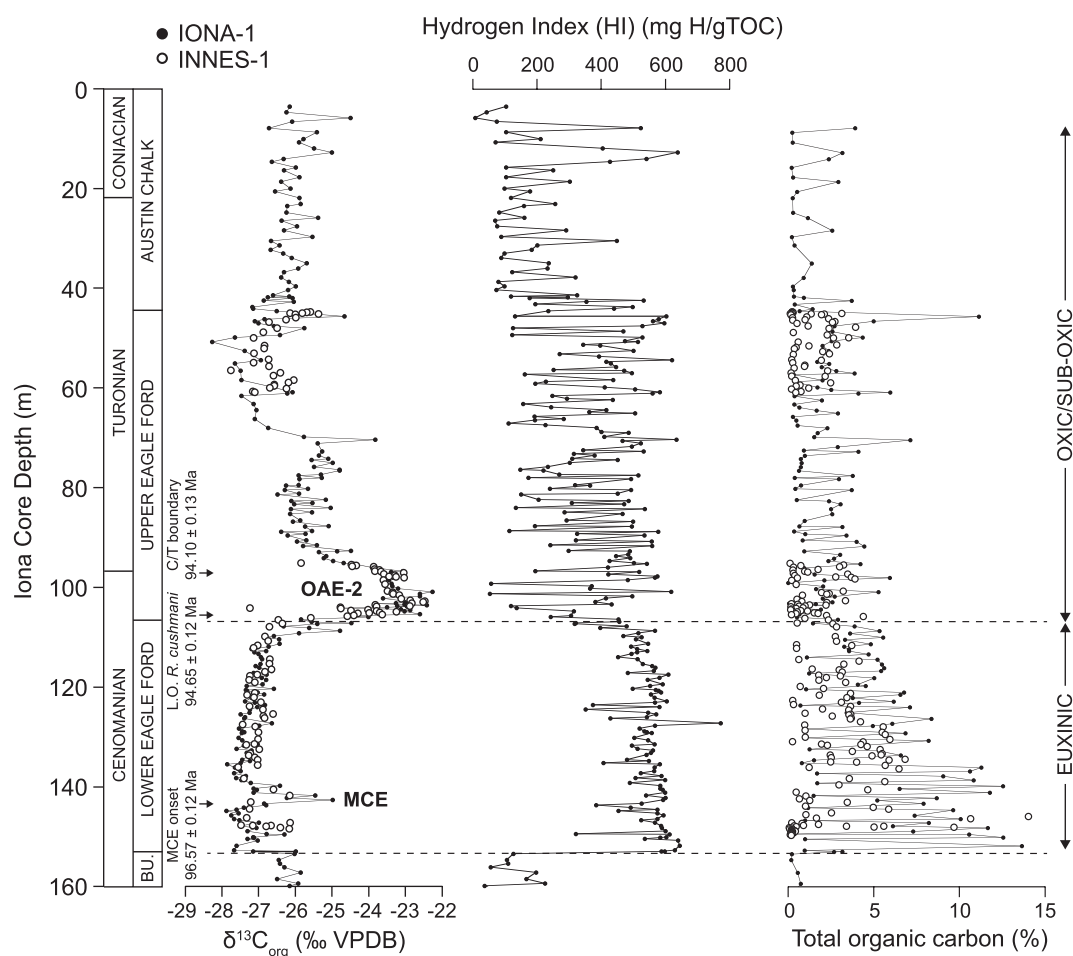


**Figure 2.** Chemostratigraphic data from the Iona-1 and Innes-1 cores. The Innes-1 data are plotted on the Iona-1 depth scale using tie-points between each core (Minisini et al., 2017). Carbon-isotope, TOC, HI data and ages are from Eldrett et al. (2014, 2015a, 2015b, 2017). MCE: Mid-Cenomanian Event. Biostratigraphic datum levels are taken from Eldrett et al. (2015a), where L.O. is defined as Last Occurrence.

## 5. Results

The average  $\delta^{98/95}\text{Mo}$  value of samples from the organic-rich LEF Group is  $0.64\% \pm 0.14\%$  (1 S.D.) for the Iona-1 core, and  $0.65\% \pm 0.15\%$  (1 S.D.) for the Innes-1 core (Figure 3). The average  $\delta^{98/95}\text{Mo}$  values of samples from the UEF Group are marginally lighter than for the LEF, at  $0.60\% \pm 0.53\%$  (1 S.D.) for the Iona-1 core and  $0.55\% \pm 0.41\%$  (1 S.D.) for the Innes-1 core but are much more variable. The more variable Mo-isotope data from the UEF occur in bioturbated marlstones and limestones with generally low Mo concentrations (Denne et al., 2014; Eldrett et al., 2014, 2015b; Lowery et al., 2014).  $\delta^{98/95}\text{Mo}$  values are unrelated to Mo concentrations, especially in the lowermost LEF where limestones containing  $\sim 5$  ppm Mo have nearly identical  $\delta^{98/95}\text{Mo}$  to stratigraphically adjacent marlstones with  $\sim 240$  ppm Mo (Figure 3).

## 6. Discussion

### 6.1. Pre OAE 2 $\delta^{98/95}\text{Mo}$

The isotopic composition of pre OAE 2 seawater needs to be estimated in order to quantify the magnitude of a Mo-isotope shift associated with OAE 2. This value can be inferred from the Maverick Basin deposits by first identifying the main carrier phases of Mo. The LEF was formed under dominantly euxinic depositional conditions, evidenced from very diverse lines of data: very high concentrations of authigenic Mo (Eldrett

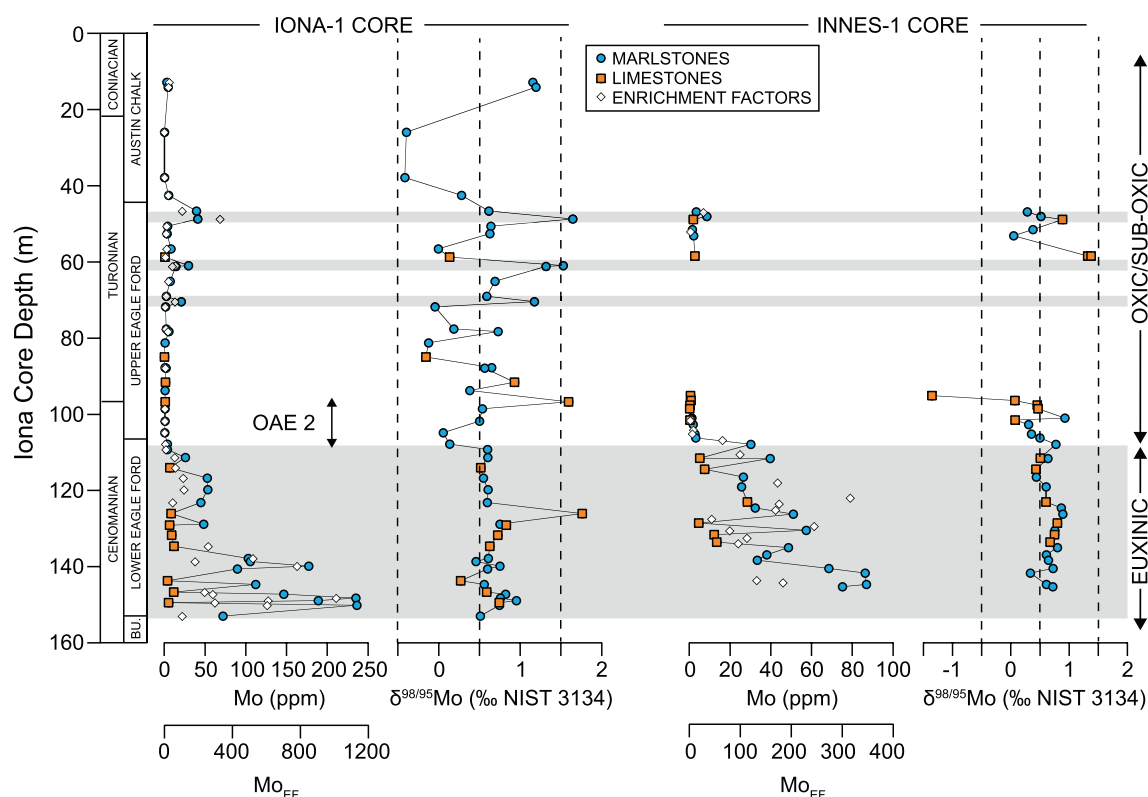


**Figure 3.**  $\delta^{98/95}\text{Mo}$  and Mo concentration data from the Iona-1 and Innes-1 cores. Data are delineated by lithology. Vertical dashed lines are to enable visual comparison between the Mo-isotope data for each core. Zones of reduced oxygenation, including the Lower Eagle Ford and intervals in the Upper Eagle Ford, are highlighted by gray shading.

et al., 2014), Cd (Sweere et al., 2020), aryl-isoprenoids derived from purple sulfur-oxidizing bacteria (Sun et al., 2016), high dibenzothiophene/phenanthrene (DBT/P) ratios that signify the incorporation of reduced sulfur into organic matter (Hughes et al., 1995; Sun et al., 2016), and the complete absence of benthic fauna (Denne et al., 2014; Lowery et al., 2014; Eldrett et al., 2015b). Mo is therefore dominantly bound as Mo-sulfides (i.e. a mixture of thiomolybdate species) in these sediments. Other Mo-hosting phases such as Mn- and Fe-oxyhydroxides and organic matter are considered minor contributors to the bulk sediment Mo. Mn is mainly enriched in carbonate beds due to the incorporation of reduced Mn(II) (Eldrett et al., 2015b) and the highest enrichments of Mo (defined as  $\text{Mo}_{\text{EF}}$ ) (>400) actually occur at levels where  $\text{Mn}_{\text{EF}}$  are lower than 1. Even in samples where  $\text{Mn}_{\text{EF}}$  and  $\text{Mo}_{\text{EF}}$  are both high (in some limestone beds, Figure 4), the  $\delta^{98/95}\text{Mo}$  compositions are similar to adjacent marlstones where  $\text{Mn}_{\text{EF}}$  is very low. Low Fe/Al ratios of  $\sim 0.5$  are close to the average continental crust (Rudnick & Gao, 2003), and are suggestive of an iron-poor setting that would not have played a dominant role in hosting Mo in the sediments (e.g., Lyons and Severmann, 2006; Figure 4). The role of organic matter as a host for Mo is debated (Dickson et al., 2019; King et al., 2018), but  $\text{Mo}_{\text{EF}}$  and TOC are only weakly correlated in the LEF samples (Figure 4). The trend of  $\text{Mo}_{\text{EF}}$  versus  $U_{\text{EF}}$  for the LEF deposits (Figure 4) follows a pattern indicative of Fe-Mn shuttling across a sharp chemocline (Algeo & Tribouillard, 2009) and supports the interpretation that the deeper parts of the Maverick Basin were corrosive to oxyhydroxide phases. Mo sulfides must therefore quantitatively account for the bulk of the authigenic Mo present in the LEF deposits. Mo enrichment factors for limestones and marls in the LEF are similar, suggesting that large variations in Mo concentrations in the LEF can be largely attributed to dilution by enhanced planktonic carbonate fluxes that formed the limestone beds (Figure S1; Eldrett et al., 2015b). The similar values and limited variance of the Mo-isotope data in the Iona-1 and Innes-1 cores shows that the sulfidic depositional conditions that governed Mo burial in the LEF were uniform at a scale of at least  $\sim 100$  km across the Maverick Basin.



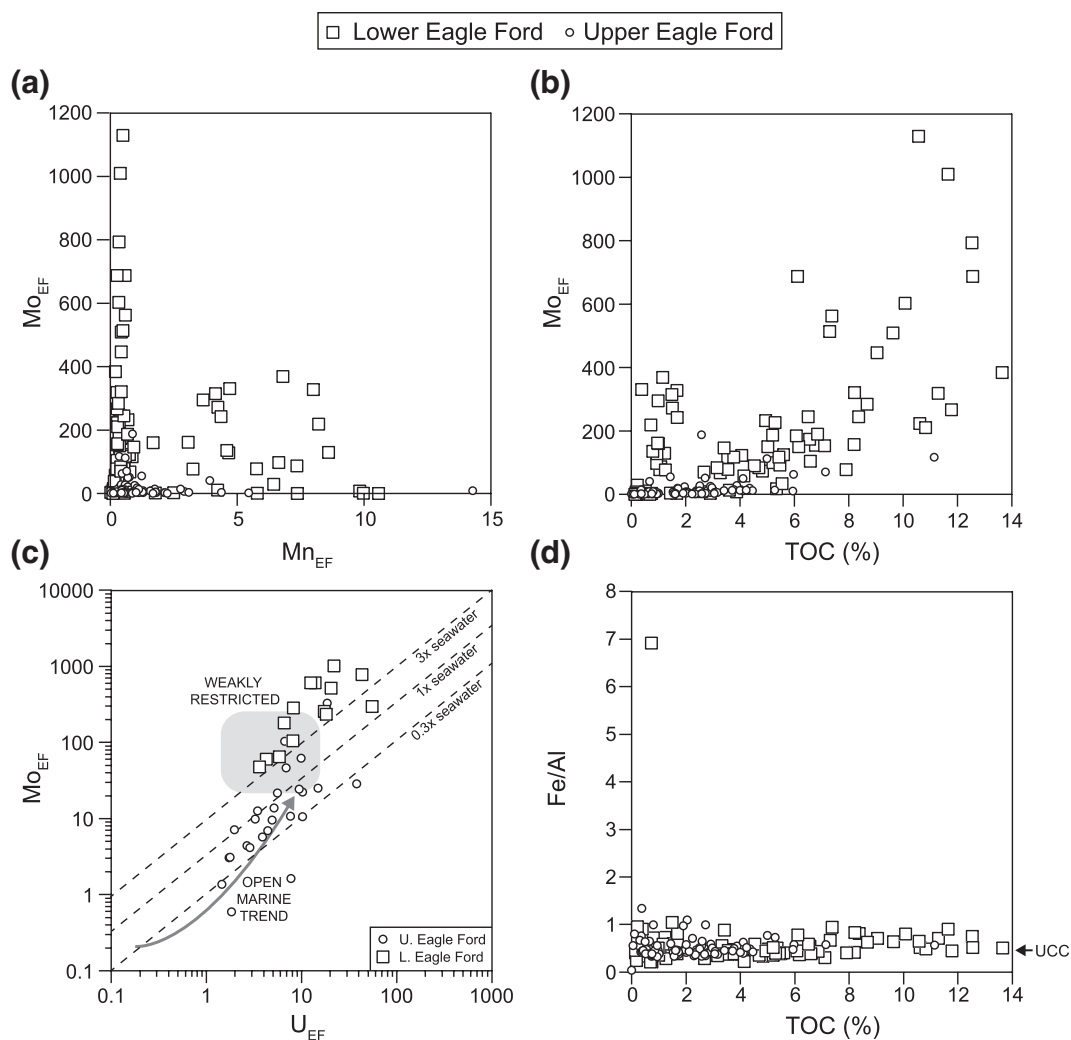


**Figure 4.** Co-variation of Mo enrichment factors with Mn<sub>EF</sub> (a), % TOC (b) and U<sub>EF</sub> (c). Panel D shows the relationship between %TOC and Fe/Al. The arrow in C indicates the typical relationship between Mo<sub>EF</sub> and U<sub>EF</sub> in open-ocean settings (Algeo & Tribovillard, 2009). The modern seawater molar Mo/U ratio is ~7.5–7.9, equating to a sedimentary mass ratio of ~3, which is shown in the figure as a dashed line. The range of Mo<sub>EF</sub> and U<sub>EF</sub> for the modern Cariaco Basin (Algeo & Tribovillard, 2009) is shown by the gray shading. The arrow in D is the Fe<sub>T</sub>/Al ratio of the Upper Continental Crust (~0.43) from Rudnick and Gao (2003).

The relationship between the Mo-isotope composition of the sediments and paleo-seawater is controlled by the distribution of Mo in sedimentary phases (which may be isotopically different) and the fraction of Mo that was removed from the water column. For the latter mechanism, a higher fraction of removal from seawater to sediments tends to increase the Mo-isotope composition of the sediments toward the seawater value. These parameters are closely tied to deep-water renewal times and the concentration of aqueous H<sub>2</sub>S (Brüske et al., 2020; Noordmann et al., 2015). For the LEF, the very high concentrations of Mo are not consistent with a limited metal supply to the Maverick Basin. A steady inflow of oxygenated near-surface waters, above the chemocline, is suggested by the presence of paleontological assemblages of Tethyan planktonic organisms in these deposits (Eldrett et al., 2017).

Similar euxinic but nonrestricted settings in the modern ocean include the Cariaco Basin, where Holocene sediments have Mo-isotope compositions of ~1‰–1.8‰, being 1.3‰ to –0.5‰ lower than modern global seawater (Brüske et al., 2020). Sediments with even lower Mo-isotope compositions occur in modern sulfidic environments where frequent basin-floor ventilation events limit H<sub>2</sub>S concentrations to levels where

isotopically light intermediate thiomolybdates form and/or a large fraction of the sediment Mo is delivered to sediment by adsorption–desorption to Fe- and Mn-oxyhydroxides (Azrieli-Tal et al., 2014; Hardisty et al., 2016; Neubert et al., 2008; Scholz et al., 2017). However, evidence for these processes operating in the Cenomanian (pre OAE 2) Maverick Basin is weak. Given the evidence for a well-developed chemocline (from  $\text{Mo}_{\text{EF}}/\text{U}_{\text{EF}}$ ) and limited Fe and Mn enrichments, it is probable that the deepest waters of the Maverick Basin did not experience frequent deep-water renewal, even while surface waters were able to exchange with the wider proto-North Atlantic. Thus, the range of offsets between the Mo-isotope compositions of Holocene sediments and modern Cariaco Basin seawater (−0.5% to −1.3%) are likely to be applicable to the LEF deposits (~0.6%). These considerations suggest a likely range of  $\delta^{98/95}\text{Mo}$  in pre OAE 2 Cenomanian seawater in the Maverick Basin of ~1.1%–1.9%. This estimate is supported by a very high value of 1.7% measured in a LEF limestone bed. Since this excursion occurred much faster than the residence time of Mo in the oceans ( $10^5$  years), we assume that local quantitative Mo removal occurred for a short period of time during deposition of this particular limestone bed (Figure 3).

Our ability to constrain global redox conditions from the Eagle Ford deposits relies on the assumption that seawater chemistry in the Maverick Basin was compositionally similar to that of the global ocean. This is not a straightforward assumption given that seawater was probably sourced from the near-surface waters of the proto-North Atlantic, where the water chemistry may have evolved away from that of the global ocean due to hydrographic restriction and intensely euxinic conditions (Dickson et al., 2016). These artifacts may for instance have influenced the Cd-isotope composition of Maverick Basin seawater (Sweere et al., 2020). Such features are not, however, likely to have been problematic for Mo. The near-surface waters flowing into the Maverick Basin would have been sourced predominantly from above the chemocline where, by analogy with the modern Black Sea, Mo concentrations and compositions would have been similar to open-ocean seawater (Nägler et al., 2011). If Mo drawdown in the proto-North Atlantic Ocean had caused local seawater  $\delta^{98/95}\text{Mo}$  to evolve slightly higher than open-ocean seawater, the values obtained from the Eagle Ford deposits would also be biased to higher values: this would only emphasize our central point (below) that there is very little evidence of a strong decrease in global seawater  $\delta^{98/95}\text{Mo}$  at the onset of OAE 2.

Upper Cenomanian sediments from DSDP Site 367 (Cape Verde Basin, eastern equatorial Atlantic) and core S57 (Tarfaya Basin, Morocco), which immediately predate the OAE 2 interval, have been well characterized by Fe-speciation, biomarkers and Mo concentrations to have been deposited in anoxic–euxinic water columns (Sinninghe Damsté & Köster, 1998; Westermann et al., 2014; Poulton et al., 2015).  $\delta^{98/95}\text{Mo}$  values reach ~0.6% at Site 367, consistent with, but marginally lower than those of the LEF (Dickson et al., 2016; Westermann et al., 2014). A difference of ~0.7% between these deposits and overlying seawater, as observed for modern (Poulson-Brucker et al., 2009) and ancient (Dickson, 2017; Dickson et al., 2014, 2016) anoxic–euxinic sedimentary deposits, would result in an estimate of Late Cenomanian Atlantic seawater of >1.3%, also within the range of estimates established from the LEF. In the Tarfaya Basin,  $\delta^{98/95}\text{Mo}$  values reach ~1.0% in core S57 (Dickson et al., 2016; Goldberg et al., 2016), approaching the lower limit of the inferred range of pre OAE 2 seawater values (1.1%–1.9%).

## 6.2. OAE 2 $\delta^{98/95}\text{Mo}$

Mo-isotope data from the OAE 2 interval of the Iona-1 and Innes-1 cores cannot be readily interpreted in terms of paleo-seawater chemistry. Oxidic depositional conditions near the base of the OAE 2 level, evidenced by low redox-sensitive metal enrichments and strongly bioturbated sediments (Eldrett et al., 2014; Sweere et al., 2020), probably led to an unknown mixture of Mo-hosting phases that were variably fractionated from seawater. However, based on biomarker data, Fe-speciation studies and trace-element patterns, the Mo-isotope composition of seawater at the peak of OAE 2 has been estimated at between 1.1% and 1.45% from high-resolution sampling of organic-rich mudrocks deposited under euxinic conditions in the Cape Verde Basin in the restricted proto-Atlantic Ocean (DSDP 367) and in the Tarfaya Basin off Morocco, (core S57), which has long been considered as a paleo-upwelling area (Dickson et al., 2016; Goldberg et al., 2016; Kolonic et al., 2005; Westermann et al., 2014; Wiedmann et al., 1978). Importantly, the higher figure (1.45%), assumed to be the closest to the true marine composition, cannot be distinguished from the range for Late Cenomanian pre OAE 2 seawater Mo-isotope ratios presented here (~1.1%–1.9%). The new data imply that

the magnitude of  $\delta^{98/95}\text{Mo}$  change during the onset of OAE 2 must have been significantly smaller than the  $\sim 0.9\%$  difference between values at the acme of OAE 2 and values of modern seawater (Dickson, 2017).

### 6.3. PostOAE 2 $\delta^{98/95}\text{Mo}$

Authigenic enrichments of Mo in the UEF deposits are considerably lower than in the LEF due to deposition under more oxygenated conditions (Eldrett et al., 2014; Minisini et al., 2017). The deposits are very different from those of the LEF: they contain a diverse benthic fauna, bioturbation structures, lower TOC and lower redox-sensitive metal concentrations, and highly variable HI values indicating generally poor organic-matter preservation (Figure 2; Boling & Dworkin, 2015; Eldrett et al., 2014; Lowery et al., 2014; Sullivan et al., 2020; Sweere et al., 2020). The interpretation of  $\delta^{98/95}\text{Mo}$  in these deposits is complicated by the variable distribution of Mo in S-, organic-, oxyhydroxide- and detrital-mineral phases.

Against a background of generally oxygenated depositional conditions of the UEF,  $\text{Mo}_{\text{EF}}$  and TOC increase to significantly higher values in several stratigraphic levels (Figures 2 and 3). These higher values may be related to the increased local availability of reduced S and thus short-term declines in the oxygenation state of the Maverick Basin. Since sediment Mo-isotope compositions are always lower than the seawater they form in, the minimum  $\delta^{98/95}\text{Mo}$  composition of Turonian seawater can be constrained by the highest isotopic values from these stratigraphic units (containing Mo concentrations of 30–40 ppm) to  $>1.6\%$  (Figure 3).

### 6.4. Evolution of Late Cretaceous Seawater $\delta^{98/95}\text{Mo}$

The inferred evolution of Late Cretaceous seawater  $\delta^{98/95}\text{Mo}$  across OAE 2 is shown in Figure 5. The change in Late Cretaceous global seawater  $\delta^{98/95}\text{Mo}$  across the onset of OAE 2 can be constrained to less than  $\sim 0.4\%$ .  $\delta^{98/95}\text{Mo}$  may have evolved to higher values after OAE 2 but the magnitude of this change cannot be tightly determined with the Eagle Ford data. The rather small change in  $\delta^{98/95}\text{Mo}$  at the onset of OAE 2 is at odds with observations of a significant expansion of euxinic conditions at a large number of locations worldwide during OAE 2 (Jenkyns, 2010; Monteiro et al., 2012; Owens et al., 2013; Pancost et al., 2004; Robinson et al., 2017; Sinninghe Damsté & Köster, 1998) that might predict a much greater change (decrease) in the Mo-isotope composition of seawater as the burial of Mo-sulfides increased. This apparent paradox could be explained if the large removal flux of Mo into spatially extensive sulfidic marine sediments was at least partly balanced by a greater removal flux of isotopically lighter Mo into nonsulfidic sediments in marine environments elsewhere. Mn-oxyhydroxides are unlikely to have constituted a major sink for Mo, since their burial flux is suggested to have decreased by  $>40\%$  near the onset of OAE 2 (Ostrander et al., 2017). The burial of isotopically light Mo in association with intermediate thiomolybdate species is possible during OAE 2 (Azrieli-Tal et al., 2014), but there is presently no observational evidence for this process.

Enhanced burial of Mo by adsorption to Fe-oxyhydroxides is, however, possible at the onset of OAE 2. There is a wealth of stratigraphic evidence that eustatic sea level rose dramatically during the latest Cenomanian into the Turonian coincident with OAE 2 (e.g., Arthur et al., 1987; Gale et al., 2002, 2008; Haq, 2014; Jones et al., 2019). The consequent transgressions would have led to the spread of low-oxygen water masses onto oxygenated continental shelves and stimulated reduction of Fe(III), followed by shuttling of Fe(II) to the open ocean and subsequent re-oxidation and burial.

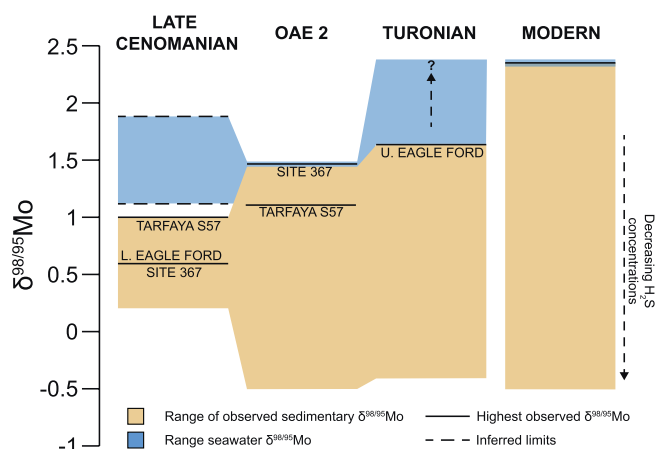


**Figure 5.** Constraints on the  $\delta^{98/95}\text{Mo}$  composition of Late Cretaceous and modern seawater. Solid horizontal lines indicate highest  $\delta^{98/95}\text{Mo}$  values observed from sediments accumulating in euxinic waters in restricted or nonrestricted marine basins (Westermann et al., 2014; Dickson et al., 2016; Goldberg et al., 2016; this study). The range of  $\delta^{98/95}\text{Mo}$  for all sediments measured in each time slice is represented by the yellow shading (Lower Cenomanian:  $0.2\%$ – $1\%$  (Site 367, S57 and Iona-1, Westermann et al., 2014; Dickson et al., 2016; Goldberg et al., 2016); OAE-2:  $-0.5\%$ – $1.5\%$ , (Site 367, S57 and Site 1,276, Westermann et al., 2014; Dickson et al., 2016; Goldberg et al., 2016); Turonian:  $-0.4\%$ – $1.6\%$  (Iona-1). The possible range of seawater  $\delta^{98/95}\text{Mo}$  for each time slice is indicated by the blue shading. Inferred limits on the range of seawater  $\delta^{98/95}\text{Mo}$  are indicated by horizontal dashed lines. The vertical dashed line indicates that the seawater composition for the Turonian extends above the highest measured sediment  $\delta^{98/95}\text{Mo}$  value by an unknown amount. The modern sediment data range is from Siebert et al., 2003, 2006; Neubert et al., 2008; Poulson-Brucker et al., 2009; Nægler et al., 2011; Nakagawa et al., 2012; Noordmann et al., 2015; Hardisty et al., 2016; Scholz et al., 2017; Brüske et al., 2020.



Although the KWIS became better oxygenated during OAE 2, there is evidence for enhanced Fe burial, ostensibly caused by diagenetic pyrite formation below the sediment–water interface (e.g., Meyers et al., 2005). Large areas of shallow continental shelf elsewhere in the oceans experienced a change toward more poorly oxygenated conditions. In the European Vocontian Basin and the Russian epi-continental shelf, moderate trace-metal and organic-matter enrichments during OAE 2 suggest a shift to suboxic to anoxic conditions, where the redoxcline probably fluctuated across the sediment–water interface (Danzelle et al., 2018; Gale et al., 2019; Gavrilov et al., 2013). Such conditions would be prone to the shuttling of Fe(II), as implied by iron-isotope data from the proto-North Atlantic region (Owens et al., 2012).

Under conditions of unusually high global paleotemperatures during OAE 2 (Jenkyns, 2018; O'Brien et al., 2017), the mass of Fe delivered to the open ocean would have been further increased by the weathering of Fe-rich terrestrial and marine silicate rocks, some of which were formed during the emplacement of the Caribbean, High Arctic and Madagascan Large Igneous Provinces (Du Vivier et al., 2014; Jenkyns et al., 2017; Pogge von Strandmann et al., 2013; Scaife et al., 2017; Turgeon & Creaser, 2008). We can roughly estimate the size of a volcanic Fe-associated Mo burial flux, albeit with large uncertainties. The amount of basalt weathered into the oceans during OAE 2 has been estimated as  $\sim 0.6\text{--}2$  million  $\text{km}^3$  using Li-isotope data (Pogge von Strandmann et al., 2013). Assuming this basalt had a density of  $2.9\text{ g cm}^{-3}$ , contained  $\sim 8\%$  Fe and was eventually buried as Fe(III)-oxides, the mass of associated Mo can be estimated from the Mo/Fe mass ratio of modern Fe-rich crusts and nodules ( $\sim 0.0015\text{--}0.0076\text{ gg}^{-1}$ ; Hein et al., 1997). Dividing the total masses by the duration of OAE 2 ( $\sim 1$  million years) results in annual burial fluxes of  $2.2 \times 10^9\text{ mol yr}^{-1}$  (minimum) to  $36.7 \times 10^9\text{ mol yr}^{-1}$  (maximum). These fluxes are  $\sim 6\text{--}110$  times larger than the modern annual input flux of Mo to the ocean (Miller et al., 2011).

Enhanced Fe burial during OAE 2 is further supported by Fe-isotope data, and the local presence of marine red beds and glauconite-rich deposits from the proto-North Atlantic, Pacific and Tethyan regions (Dickson et al., 2017; Gale et al., 2019; Gangl et al., 2019; Hasegawa et al., 2013; Jenkyns, 1980; Owens et al., 2012; Takashima et al., 2011; Wohlwend et al., 2015). Assuming that these burial fluxes had isotopic compositions as much as 2.2% lower than coeval seawater, they would have been capable of balancing similarly high Mo-S burial fluxes and contributing to large-scale drawdown of oceanic Mo during OAE 2.

### 6.5. Behavior of Other Redox-Sensitive Metal-Isotope Systems

The small range of seawater  $\delta^{98/95}\text{Mo}$  variability detailed here for the Late Cretaceous implies that for metal-isotope systems such as Mo it is difficult to accurately estimate the areal extent of euxinia unless the influence of all burial fluxes on the global mass balance are fully understood. For OAE 2, U isotopes (Clarkson et al., 2018) and Zn isotopes (Sweere et al., 2018) also show remarkably muted changes compared to Late Cenomanian background compositions. In both cases, significant metal-isotope variability was registered during OAE 2 rather than at its onset or termination, specifically during the so-called Plenus Cold Event, an interval of regionally modulated cooling and re-oxygenation of ocean waters (Boundinot & Sepúlveda, 2020; Jenkyns et al., 2017; O'Connor et al., 2020). These geochemical changes, a negative excursion in the case of Zn, a positive excursion in the case of U, can be related to the isotopically distinct behavior of these elements during burial in reducing and oxidizing sedimentary environments and the consequent effect on ocean chemistry. Thus, just as for Mo, their global behavior may have become significantly affected by the impact of other biogeochemical cycles (e.g., an increased supply of Fe addition to the oceans) at times of rapid global redox change.

## 7. Conclusion

New Mo-isotope data from the Eagle Ford Group of South Texas, USA, constrain the isotopic composition of Middle to Late Cenomanian seawater ( $\sim 96.5\text{--}94$  Ma, prior to OAE 2) to a range ( $\sim 1.1\%\text{--}1.9\%$ ) that is notably lower than the present-day composition of  $\sim 2.3\%$ . The relative stability of this value over  $\sim 2.5$  million years indicates that Late Cretaceous oceans had a greater extent of euxinic seafloor than exists today. The new data limit the range by which the Mo-isotope composition of seawater in the Maverick Basin, and by extension the global ocean, could have evolved during OAE 2 to less than  $\sim 0.4\%$ . This limited range plausi-

bly records the balancing of Mo burial into sulfidic sediments against Mo burial associated with Fe-oxyhydroxides, although the impact of thiomolybdate removal in weakly sulfidic sediments cannot be presently excluded. High Fe fluxes are a probable consequence of relatively expanded shelf seas with only partially deoxygenated sediments during a major global sea-level highstand, alongside the rapid weathering of Fe from newly emplaced Large Igneous Province basalts. These results highlight significant complexity with the interpretation of Mo, and other redox-sensitive isotope systems such as Zn and U, across an interval of very rapid environmental change associated with intensive volcanic activity and one of the highest sea levels of the Late Phanerozoic (Gale et al, 2002, 2008; Hancock and Kaufmann, 1979; Haq, 2014; Jenkyns et al., 2017; Turgeon & Creaser, 2008).

## Data Availability Statement

Raw data are available in the Supplementary Information and from the Pangaea database ([doi.pangaea.de/10.1594/PANGAEA.926793](https://doi.org/10.1594/PANGAEA.926793)).

## Acknowledgments

The authors wish to thank James Scaife, Steve Bergman and Daniel Minisini for help sampling the Iona-1 and Innes-1 cores, and Alan Hsieh and Steve Wyatt for laboratory assistance. This work was funded by Shell Global Solutions International B.V.

## References

- Algeo, T. J., & Tribouillard, N. (2009). Environmental analysis of paleoceanographic systems based on molybdenum-uranium covariation. *Chemical Geology*, 268, 211–225. <https://doi.org/10.1016/j.chemgeo.2009.09.001>
- Arthur, M. A., Jenkyns, H. C., Brumsack, H.-J., & Schlanger, S. O. (1990). Stratigraphy, geochemistry, and paleoceanography of organic carbon-rich Cretaceous sequences. In R. N. Ginsburg, & B. Beaudoin (Eds.), *Cretaceous resources, events and rhythms*. NATO ASI ser. C (Vol. 304, pp. 75–119). Dordrecht: Kluwer Academic Publishers. <https://doi.org/10.1007/978-94-015-6861-6/6>
- Arthur, M. A., & Sageman, B. (1994). Marine black shales: depositional mechanisms and environments of ancient deposits. *Annual Review of Earth and Planetary Sciences*, 22, 499–551. <https://doi.org/10.1146/annurev.ea.22.050194.002435>
- Arthur, M. A., Schlanger, S. O., & Jenkyns, H. C. (1987). The Cenomanian–Turonian Oceanic Anoxic Event, II. Paleocceanographic controls on organic-matter production and preservation. In J. Brooks, & A. J. Fleet (Eds.), *Marine petroleum source rocks* (Vol. 26, pp. 401–420). London: Special Publication Geological Society. <https://doi.org/10.1144/GSL.SP.1987.026.01.25>
- Azrieli-Tal, I., Bar-Matthews, M., Almogi-Labin, A., Vance, D., Archer, C., & Teutsch, N. (2014). Evidence from molybdenum and iron isotopes and molybdenum-uranium covariation for sulphidic bottom waters during Eastern Mediterranean sapropel S1 formation. *Earth and Planetary Science Letters*, 393, 231–242. <https://doi.org/10.1016/j.epsl.2014.02.054>
- Barling, J., & Anbar, A. D. (2004). Molybdenum isotope fractionation during adsorption by manganese oxides. *Earth and Planetary Science Letters*, 217, 315–329. [https://doi.org/10.1016/S0012-821X\(03\)00608-3](https://doi.org/10.1016/S0012-821X(03)00608-3)
- Boling, K. S., & Dworkin, S. I. (2015). Origin of organic matter in the Eagle Ford Formation. *Interpretation*, 3, 27–39. <https://doi.org/10.1190/INT-2014-0103.1>
- Boundinot, F. G., & Sepúlveda, J. (2020). Marine organic carbon burial increased forest fire frequency during Oceanic Anoxic Event 2. *Nature Geoscience*, 13, 693–698. <https://doi.org/10.1038/s41561-020-0633-y>
- Brüske, A., Weyer, S., Zhao, M.-Y., Planavsky, N. J., Wegworth, A., Neubert, N., et al. (2020). Correlated molybdenum and uranium isotope signatures in modern anoxic sediments: Implications for their use as paleo-redox proxy. *Geochimica et Cosmochimica Acta*, 270, 449–474. <https://doi.org/10.1016/j.gca.2019.11.031>
- Chen, X., Ling, H.-F., Vance, D., Shields-Zhou, G. A., Zhu, M., Poulton, S. W., et al. (2015). Rise to modern levels of ocean oxygenation coincided with the Cambrian radiation of animals. *Nature Communications*, 6, 7142. <https://doi.org/10.1038/ncomms8142>
- Clarkson, M. O., Stirling, C. H., Jenkyns, H. C., Dickson, A. J., Porcelli, D., Moy, C. M., et al. (2018). Uranium isotope evidence for two episodes of deoxygenation during Oceanic Anoxic Event 2. *Proceedings of the National Academy of Sciences of the United States of America*, 115, 2918–2923. <https://doi.org/10.1073/pnas.1715278115>
- Dahl, T. W., Chappaz, A., Hoek, J., McKenzie, C. J., Svane, S., & Canfield, D. E. (2017). Evidence of molybdenum association with particulate organic matter under sulfidic conditions. *Geobiology*, 15, 311–323. <https://doi.org/10.1111/gbi.12220>
- Danzelle, J., Riquier, L., Baudin, F., Thomazo, C., & Pucéat, E. (2018). Oscillating redox conditions in the Vocontian Basin (SE France) during Oceanic Anoxic Event 2 (OAE 2). *Chemical Geology*, 493, 136–152. <https://doi.org/10.1016/j.chemgeo.2018.05.039>
- Denne, R. A., Hinote, R. E., Breyer, J. A., Kosanke, T. H., Lees, J. A., Engelhardt-Moore, N., et al. (2014). The Cenomanian–Turonian Eagle Ford Group of South Texas: Insights on timing and paleoceanographic conditions from geochemistry and micropaleontologic analyses. *Palaeogeography, Palaeoclimatology, Palaeoecology*, 413, 2–28. <https://doi.org/10.1016/j.palaeo.2014.05.029>
- Dickson, A. J. (2017). A molybdenum-isotope perspective on Phanerozoic deoxygenation events. *Nature Geoscience*, 10, 721–726. <https://doi.org/10.1038/NGEO3028>
- Dickson, A. J., Cohen, A. S., & Coe, A. L. (2014). Continental margin molybdenum isotope signatures from the Early Eocene. *Earth and Planetary Science Letters*, 404, 389–395. <https://doi.org/10.1016/j.epsl.2014.08.004>
- Dickson, A. J., Idiz, E., Porcelli, D., & van den Boorn, S. H. J. M. (2019). The influence of thermal maturity on the stable isotope compositions and concentrations of molybdenum, zinc and cadmium in organic-rich marine mudrocks. *Geochimica et Cosmochimica Acta*, 287, 205–220. <https://doi.org/10.1016/j.gca.2019.11.001>
- Dickson, A. J., Jenkyns, H. C., Porcelli, D., van den Boorn, S., & Idiz, E. (2016). Basin-scale controls on the molybdenum-isotope composition of seawater during Oceanic Anoxic Event 2 (Late Cretaceous). *Geochimica et Cosmochimica Acta*, 178, 291–306. <https://doi.org/10.1016/j.gca.2015.12.036>
- Dickson, A. J., Saker-Clark, M., Jenkyns, H. C., Bottini, C., Erba, E., Russo, F., et al. (2017). A southern hemisphere record of global trace-metal drawdown and orbital modulation of organic-matter burial across the Cenomanian–Turonian boundary (Ocean Drilling Program Site 1138, Kerguelen Plateau). *Sedimentology*, 64, 186–203. <https://doi.org/10.1111/sed.12303>

- Du Vivier, A. D., Selby, D., Sageman, B. B., Jarvis, I., Gröcke, D. R., & Voigt, S. (2014). Marine  $^{187}\text{Os}/^{188}\text{Os}$  isotope stratigraphy reveals the interaction of volcanism and ocean circulation during Oceanic Anoxic Event 2. *Earth and Planetary Science Letters*, 389, 23–33. <https://doi.org/10.1016/j.epsl.2013.12.024>
- Eldrett, J. S., Dodsworth, P., Bergman, S. C., Wright, M., & Minisini, D. (2017). Water-mass evolution in the Cretaceous Western Interior Seaway of North American and equatorial Atlantic. *Climate of the Past*, 13, 855–878. <https://doi.org/10.5194/cp-13-855-2017>
- Eldrett, J. S., Ma, C., Bergman, S. C., Lutz, B., Gregory, F. J., Dodsworth, P., et al. (2015a). An astronomically calibrated stratigraphic of the Cenomanian, Turonian and earliest Coniacian from the Cretaceous Western Interior Seaway, USA: implications for global chronostratigraphy. *Cretaceous Research*, 56, 316–344. <https://doi.org/10.1016/j.cretres.2015.04.010>
- Eldrett, J. S., Ma, C., Bergman, S. C., Ozkan, A., Minisini, D., Lutz, B., et al. (2015b). Origin of limestone-marlstone cycles: astronomic forcing of organic-rich sedimentary rocks from the Cenomanian to early Coniacian of the Cretaceous Western Interior Seaway. *Earth and Planetary Science Letters*, 423, 98–113. <https://doi.org/10.1016/j.epsl.2015.04.026>
- Eldrett, J. S., Minisini, D., & Bergman, S. C. (2014). Decoupling of the carbon cycle during Ocean Anoxic Event 2. *Geology*, 42, 567–570. <https://doi.org/10.1130/G35520.1>
- Gale, A. S., Hardenbol, J., Hathway, B., Kennedy, W. J., Young, J. R., & Phansalkar, V. (2002). Global correlation of Cenomanian (Upper Cretaceous) sequences: Evidence for Milankovitch control on sea level. *Geology*, 30, 291–294. [https://doi.org/10.1130/0091-7613\(2002\)030<0291:GCOCUC>2.0.CO;2](https://doi.org/10.1130/0091-7613(2002)030<0291:GCOCUC>2.0.CO;2)
- Gale, A. S., Jenkyns, H. C., Tsikos, H., van Breugel, Y., Sinninghe Damsté, J. S., Bottini, C., et al. (2019). High-resolution bio- and chemostratigraphy of an expanded record of Oceanic Anoxic Event 2 (Late Cenomanian–Early Turonian) at Clot Chevalier, near Barrême, SE France (Vocontian Basin, SE France). *Newsletters on Stratigraphy*, 52, 97–129. <https://doi.org/10.1127/nos/2018/0445>
- Gale, A. S., Voigt, S., Sageman, B. B., & Kennedy, W. J. (2008). Eustatic sea-level record for the Cenomanian (Late Cretaceous): Extension to the Western Interior Basin, USA. *Geology*, 36, 859–862. <https://doi.org/10.1130/G24838a.1>
- Gangl, S. K., Moy, C. M., Stirling, C. H., Jenkyns, H. C., Crampton, J. S., Clarkson, M. O., et al. (2019). High-resolution records of Oceanic Anoxic Event 2: Insights into the timing, duration and extent of environmental perturbations from the palaeo-South Pacific Ocean. *Earth and Planetary Science Letters*, 518, 172–182. <https://doi.org/10.1016/j.epsl.2019.04.028>
- Gavrilov, Y. O., Shcherbinina, E. A., Golovanova, O. V., & Pokrovskii, B. G. (2013). The Late Cenomanian paleoecological event (OAE 2) in the Eastern Caucasus Basin of northern Peri-Tethys. *Lithology and Mineral Resources*, 48, 457–488. <https://doi.org/10.1134/S0024490213060047>
- Goldberg, T., Archer, C., Vance, D., & Poulton, S. W. (2009). Mo isotope fractionation during adsorption to Fe (oxyhydr)oxides. *Geochimica et Cosmochimica Acta*, 73, 6502–6516. <https://doi.org/10.1016/j.gca.2009.08.004>
- Goldberg, T., Gordon, G. W., Izon, G., Archer, C., Pearce, C. R., McManus, J., et al. (2013). Resolution of inter-laboratory discrepancies in Mo isotope data: An intercalibration. *Journal of Analytical Atomic Spectrometry*, 28, 724–735. <https://doi.org/10.1039/C3JA30375F>
- Goldberg, T., Poulton, S. W., Wagner, T., Kolonic, S., & Rehkämper, M. (2016). Molybdenum drawdown during Cretaceous Oceanic Anoxic Event 2. *Earth and Planetary Science Letters*, 440, 81–91. <https://doi.org/10.1016/j.epsl.2016.02.006>
- Hancock, J. M., & Kauffman, E. G. (1979). The great transgressions of the Late Cretaceous. *Journal of the Geological Society*, 136, 175–186. <https://doi.org/10.1144/gsjgs.136.2.0175>
- Haq, B. U. (2014). Cretaceous eustasy revisited. *Global and Planetary Change*, 113, 44–58. <https://doi.org/10.1016/j.gloplacha.2013.12.007>
- Hardisty, D. S., Riedinger, N., Planavsky, N. J., Asael, D., Andrén, T., Jørgensen, B. B., & Lyons, T. W. (2016). A Holocene history of dynamic water column redox conditions in the Landsort Deep, Baltic Sea. *American Journal of Science*, 316, 713–745. <https://doi.org/10.2475/08.2016.01>
- Hasegawa, T., Crampton, J. S., Schioler, P., Field, B., & Fukuski, K. (2013). Carbon isotope stratigraphy and depositional oxia through Cenomanian/Turonian boundary sequences (Upper Cretaceous) in New Zealand. *Cretaceous Research*, 40, 61–80. <https://doi.org/10.1016/j.jafrearsci.2014.03.003>
- Hein, J. R., Koschinsky, A., Halbach, P., Manheim, F. T., Bau, M., Kang, J.-K., & Lubick, N. (1997). Iron and manganese oxide mineralization in the Pacific. In K. Nicholson, J. R. Hein, B. Bühn, & S. Dasgupta (Eds.), *Manganese mineralization: Geochemistry and mineralogy of terrestrial and marine deposits* (Vol. 119, pp. 123–138). Geological Society Special Publication. <https://doi.org/10.1144/GSL.SP.1997.119.01.09>
- Helz, G. R., Bura-Nakić, E., Mikac, N., & Ciglenečki, I. (2011). New model for molybdenum behavior in euxinic waters. *Chemical Geology*, 284, 323–332. <https://doi.org/10.1016/j.chemgeo.2011.03.012>
- Helz, G. R., Miller, C. V., Charnock, J. M., Mosselmans, J. F. W., Pattrick, R. A. D., Garner, C. D., & Vaughan, D. J. (1996). Mechanism of molybdenum removal from the sea and its concentration in black shales: EXAFS evidence. *Geochimica et Cosmochimica Acta*, 60, 3631–3642. [https://doi.org/10.1016/0016-7037\(96\)00195-0](https://doi.org/10.1016/0016-7037(96)00195-0)
- Hetzel, A., Böttcher, M. E., Wortmann, U. G., & Brumsack, H.-J. (2009). Paleo-redox conditions during OAE 2 reflected in Demerara Rise sediment geochemistry (ODP Leg 207). *Palaeogeography, Palaeoclimatology, Palaeoecology*, 273, 302–328. <https://doi.org/10.1016/j.palaeo.2008.11.005>
- Hughes, W. B., Holba, A. G., & Dzou, L. I. P. (1995). The ratios of dibenzothiophene to phenanthrene and pristane to phytane as indicators of depositional environment and lithology of petroleum source rocks. *Geochimica et Cosmochimica Acta*, 59, 3581–3598. [https://doi.org/10.1016/0016-7037\(95\)00225-0](https://doi.org/10.1016/0016-7037(95)00225-0)
- Hutchings, A. M., Basu, A., Dickson, A. J., & Turchyn, A. V. (2020). Molybdenum geochemistry in salt marsh pond sediments. *Geochimica et Cosmochimica Acta*, 284, 75–91. <https://doi.org/10.1016/j.gca.2020.06.014>
- Ito, T., Nenes, A., Johnson, M. S., Meskhidze, N., & Deutsch, C. (2016). Acceleration of oxygen decline in the tropical Pacific over the past decades by aerosol pollutants. *Nature Geoscience*, 9, 443–448. <https://doi.org/10.1038/ngeo2717>
- Jenkyns, H. C. (1980). Cretaceous anoxic events: From continents to oceans. *Journal of the Geological Society*, 137, 171–188. <https://doi.org/10.1144/gsjgs.137.2.0171>
- Jenkyns, H. C. (2010). Geochemistry of oceanic anoxic events. *Geochemistry, Geophysics, Geosystems*, 11, Q03004. <https://doi.org/10.1029/2009GC002788>
- Jenkyns, H. C. (2018). Transient cooling episodes during Cretaceous Oceanic Anoxic Events with special reference to OAE 1a (Early Aptian). *Philosophical Transactions of the Royal Society A*, 376, 20170073. <https://doi.org/10.1098/rsta.2017.0073>
- Jenkyns, H. C., Dickson, A. J., Ruhl, M., & van den Boorn, S. H. J. M. (2017). Basalt–seawater interaction, the Plenus Cold Event, enhanced weathering and geochemical change: Deconstructing Oceanic Anoxic Event 2 (Cenomanian–Turonian, Late Cretaceous). *Sedimentology*, 64, 16–43. <https://doi.org/10.1111/sed.12305>
- Jones, M. M., Sageman, B. B., Oakes, R. L., Parker, A. L., Leckie, R. M., Bralower, T. J., et al. (2019). Astronomical pacing of relative sea level during Oceanic Anoxic Event 2: Preliminary studies of the expanded SH# 1 Core, *The Geological Society of America Bulletin*, 131, 1702–1722. <https://doi.org/10.1130/B32057.1>

- Keeling, R. F., Körtzinger, A., & Gruber, N. (2010). Ocean deoxygenation in a warming world. *Annual Review of Marine Science*, 2, 199–229. <https://doi.org/10.1146/annurev.marine.010908.163855>
- Kendall, B., Dahl, T. W., & Anbar, A. D. (2017). Good golly why moly? The stable isotope geochemistry of molybdenum. *Reviews in Mineralogy and Geochemistry*, 82, 683–732. <https://doi.org/10.2138/rmg.2017.82.16>
- King, E. K., Perakis, S. S., & Pett-Ridge, J. C. (2018). Molybdenum isotope fractionation during adsorption to organic matter. *Geochimica et Cosmochimica Acta*, 222, 584–598. <https://doi.org/10.1016/j.gca.2017.11.014>
- King, E. K., & Pett-Ridge, J. C. (2018). Reassessing the dissolved molybdenum isotopic composition of ocean inputs: The effect of chemical weathering and groundwater. *Geology*, 46, 955–958. <https://doi.org/10.1130/G45124.1>
- Kolonis, S., Wagner, T., Forster, A., Sinninghe Damsté, J. S., Walsworth-Bell, B., Erba, E., et al. (2005). Black shale deposition on the north-west African Shelf during the Cenomanian/Turonian oceanic anoxic event: Climate coupling and global organic carbon burial. Astronomical constraints on global carbon-cycle perturbation during Oceanic Anoxic Event 2 (OAE2). *Paleoceanography*, 20, PA100635–46. <https://doi.org/10.1029/2003PA000950>
- Li, Y. X., Montañez, I. P., Liu, Z., & Ma, L. (2017). Astronomical constraints on global carbon-cycle perturbation during Oceanic Anoxic Event 2 (OAE2). *Earth and Planetary Science Letters*, 462, 35–46.
- Lowery, C. M., Corbett, M. J., Leckie, R. M., Watkins, D., Miceli Romero, A., & Pramudito, A. (2014). Foraminiferal and nannofossil paleoecology and paleoceanography of the Cenomanian–Turonian Eagle Ford Shale of Southern Texas. *Paleogeography, Paleoclimatology, Palaeoecology*, 413, 49–65. <https://doi.org/10.1016/j.palaeo.2014.07.025>
- Lyons, T. W., & Severmann, S. (2006). A critical look at iron paleoredox proxies: new insights from modern euxinic marine basins. *Geochimica et Cosmochimica Acta*, 70, 5698–5722.
- Meyers, S. R., Sageman, B. B., & Arthur, M. A. (2012b). Oblivious forcing of organic matter accumulation during Oceanic Anoxic Event 2. *Paleoceanography*, 27, PA3212. <https://doi.org/10.1029/2012PA002286>
- Meyers, S. R., Sageman, B. B., & Lyons, T. W. (2005). Organic carbon burial rate and the molybdenum proxy: theoretical framework and application to oceanic anoxic event 2. *Paleoceanography*, 20, PA2002. <https://doi.org/10.1029/2004PA001068>
- Meyers, S. R., Siewert, S. E., Singer, B. S., Sageman, B. B., Condon, D. J., Obradovich, J. D., et al. (2012a). Intercalibration of radioisotopic and astrochronologic time scales for the Cenomanian–Turonian boundary interval, Western Interior Basin, USA. *Geology*, 40, 7–10. <https://doi.org/10.1130/G32261.1>
- Miller, C. A., Peucker-Ehrenbrink, B., Walker, B. D., & Marcantonio, F. (2011). Re-assessing the surface cycling of molybdenum and rhenium. *Geochimica et Cosmochimica Acta*, 75, 7146–7179. <https://doi.org/10.1016/j.gca.2011.09.005>
- Minisini, D., Eldrett, J. S., Bergman, S. C., & Forkner, R. (2017). Chronostratigraphic framework and depositional environments in the organic-rich, mudstone-dominated Eagle Ford Group, Texas, USA. *Sedimentology*, 65, 1520–1557. <https://doi.org/10.1111/sed.12437>
- Monteiro, F. M., Pancost, R. D., Ridgwell, A., & Donnadieu, Y. (2012). Nutrients as the dominant control on the spread of anoxia and euxinia across the Cenomanian–Turonian oceanic anoxic event (OAE2): Model-data comparison. *Paleoceanography*, 27, PA4209. <https://doi.org/10.1029/2012PA002351>
- Montoya-Pino, C., Weyer, S., Anbar, A. D., Pross, J., Oschmann, W., van de Schootbrugge, B., & Arz, H. W. (2010). Global enhancement of ocean anoxia during Oceanic Anoxic Event 2: a quantitative approach using U isotopes. *Geology*, 38, 315–318.
- Näglér, T. F., Anbar, A. D., Archer, C., Goldberg, T., Gordon, G. W., Greber, N. D., et al. (2014). Proposal for an international molybdenum isotope measurement standard and data representation. *Geostandards and Geoanalytical Research*, 38, 149–151. <https://doi.org/10.1111/j.1751-908X.2013.00275.x>
- Näglér, T. F., Neubert, N., Böttcher, M. E., Dellwig, O., & Schnetger, B. (2011). Molybdenum isotope fractionation in pelagic euxinia: Evidence from the modern Black and Baltic Seas. *Chemical Geology*, 289, 1–11. <https://doi.org/10.1016/j.chemgeo.2011.07.001>
- Nakagawa, Y., Takano, S., Lutfi Firdaus, M., Norisuye, K., Hirata, T., Vance, D., & Sohrin, Y. (2012). The molybdenum isotopic composition of the modern ocean. *Geochemical Journal*, 46, 131–141. <https://doi.org/10.2343/geochemj.1.0158>
- Neely, R. A., Gislason, S. R., Ólafsson, M., McCoy-West, A. J., Pearce, C. R., & Burton, K. W. (2018). Molybdenum isotope behavior in groundwaters and terrestrial hydrothermal systems, Iceland. *Earth and Planetary Science Letters*, 486, 108–118. <https://doi.org/10.1016/j.epsl.2017.11.053>
- Neubert, N., Näglér, T. F., & Böttcher, M. E. (2008). Sulfidity controls molybdenum isotope fractionation into euxinic sediments: Evidence from the modern Black Sea. *Geology*, 36, 775–778. <https://doi.org/10.1130/G24959A.1>
- Noordmann, J., Weyer, S., Montoya-Pina, C., Dellwig, O., Neubert, N., Eckert, S., et al. (2015). Uranium and molybdenum isotope systematics in modern euxinic basins: Case studies from the central Baltic Sea and the Kylaren fjord (Norway). *Chemical Geology*, 396, 182–195. <https://doi.org/10.1016/j.chemgeo.2014.12.012>
- O'Connor, L. K., Jenkyns, H. C., Robinson, S. A., Remmelzwaal, S. R., Batenburg, S. J., Parkinson, I. J., & Gale, A. S. (2020). A re-evaluation of the Plenian Cold Event, and the links between CO<sub>2</sub>, temperature, and seawater chemistry during OAE 2. *Paleoceanography and Paleoclimatology*, 35, e2019PA003631. <https://doi.org/10.1029/2019PA003631>
- Ostrander, C. M., Owens, J. D., & Nielsen, S. G. (2017). Constraining the rate of oceanic deoxygenation leading up to a Cretaceous Oceanic Anoxic Event (OAE-2: ~94 Ma). *Science Advances*, 3, e1701020. <https://doi.org/10.1126/sciadv.1701020>
- Owens, J. D., Gill, B. C., Jenkyns, H. C., Bates, S. M., Severmann, S., Kuypers, M. M., et al. (2013). Sulfur isotopes track the global extent and dynamics of euxinia during Cretaceous Oceanic Anoxic Event 2. *Proceedings of the National Academy of Sciences*, 110, 18407–18412. <https://doi.org/10.1073/pnas.1305304110>
- Owens, J. D., Lyons, T. W., Li, X., Macleod, K. G., Gordon, G., Kuypers, M. M., et al. (2012). Iron isotope and trace metal records of iron cycling in the proto-North Atlantic during the Cenomanian–Turonian oceanic anoxic event (OAE 2). *Paleoceanography and Paleoclimatology*, 27, PA3223. <https://doi.org/10.1029/2012PA002328>
- Owens, J. D., Reinhard, C. T., Rohrsen, M., Love, G. L., & Lyons, T. W. (2016). Empirical links between trace metal cycling and marine microbial ecology during a large perturbation to Earth's carbon cycle. *Earth and Planetary Science Letters*, 449, 407–417. <https://doi.org/10.1016/j.epsl.2016.05.046>
- O'Brien, C. L., Robinson, S. A., Pancost, R. D., Sinninghe Damsté, J. S., Schouten, S., Lunt, D. J., et al. (2017). Cretaceous sea-surface temperature evolution: Constraints from TEX<sub>86</sub> and planktonic foraminiferal oxygen isotopes. *Earth-Science Reviews*, 172, 224–247. <https://doi.org/10.1016/j.earscirev.2017.07.012>
- Pancost, R. D., Crawford, N., Magness, S., Turner, A., Jenkyns, H. C., & Maxwell, J. R. (2004). Further evidence for the development of photic-zone euxinic conditions during Mesozoic oceanic anoxic events. *Journal of the Geological Society*, 161, 353–364. <https://doi.org/10.1144/0016764903-059>



- Pearce, C. R., Cohen, A. S., & Parkinson, I. J. (2010). Quantitative separation of molybdenum and rhenium from geological materials for isotopic determination by MC-ICP-MS. *Geostandards and Geoanalytical Research*, 33, 219–229. <https://doi.org/10.1111/j.1751-908X.2009.00012.x>
- Pogge von Strandmann, P. A. E., Jenkyns, H. C., & Woodfine, R. G. (2013). Lithium isotope evidence for enhanced weathering during Oceanic Anoxic Event 2. *Nature Geoscience*, 6, 668–672. <https://doi.org/10.1038/ngeo1875>
- Poulson-Brucker, R. L., McManus, J., Severmann, S., & Berelson, W. M. (2009). Molybdenum behavior during early diagenesis: Insights from Mo isotopes. *Geochemistry, Geophysics, Geosystems*, 10, Q06010. <https://doi.org/10.1029/2008GC002180>
- Robinson, S. A., Heimhofer, U., Hesselbo, S. P., & Petrizzo, M. R. (2017). Mesozoic climates and oceans: A tribute to Hugh Jenkyns and Helmut Weissert. *Sedimentology*, 64, 1–15. <https://doi.org/10.1111/sed.12349>
- Rudnick, R. L., & Gao, S. (2003). In D. H. Heinrich, & K. T. Karl (Eds.), *Composition of the continental crust*, *Treatise on Geochemistry* (Vol. 3, pp. 1–64). Oxford, U.K.: Pergamon. <https://doi.org/10.1016/B0-08-043751-6/03016-4>
- Sageman, B. B., Meyers, S. R., & Arthur, M. A. (2006). Orbital time scale and new C-isotope record for Cenomanian–Turonian boundary stratotype. *Geology*, 34, 125–128. <https://doi.org/10.1130/G22074.1>
- Scaife, J. D., Ruhl, M., Dickson, A. J., Mather, T. A., Jenkyns, H. C., Percival, L. M. E., et al. (2017). Sedimentary mercury enrichments as a marker for submarine large igneous province volcanism? Evidence from the mid-Cenomanian Event and Oceanic Anoxic Event 2 (Late Cretaceous). *Geochemistry, Geophysics, Geosystems*, 18, 4253–4275. <https://doi.org/10.1002/2017GC007153>
- Schlanger, S. O., Arthur, M. A., Jenkyns, H. C., & Scholle, P. A. (1987). The Cenomanian–Turonian Oceanic Anoxic Event, I. Stratigraphy and distribution of organic carbon-rich beds and the marine  $\delta^{13}\text{C}$  excursion. In J. Brooks, & A. J. Fleet (Eds.), *Marine petroleum source rocks* (Vol. 26, pp. 371–399). London: Special Publication Geological Society. <https://doi.org/10.1144/GSL.SP.1987.026.01.24>
- Schlanger, S. O., & Jenkyns, H. C. (1976). Cretaceous oceanic anoxic events: Causes and consequences. *Geologie en Mijnbouw*, 55, 179–184. <https://ora.ox.ac.uk/objects/uuid:0921605b-4793-43df-889d-7b896790de62>
- Schmitko, S., Stramma, L., & Visbeck, M. (2017). Decline in global oceanic oxygen content during the past five decades. *Nature*, 542, 335–339. <https://doi.org/10.1038/nature21399>
- Scholz, F., Siebert, C., Dale, A. W., & Frank, M. (2017). Intense molybdenum accumulation in sediments underneath a nitrogenous water column and implications for the reconstruction of paleo-redox conditions based on molybdenum isotopes. *Geochimica et Cosmochimica Acta*, 213, 400–417. <https://doi.org/10.1016/j.gca.2017.06.048>
- Shephard, J. G., Brewer, P. G., Oschiles, A., & Watson, A. J. (2017). Ocean ventilation and deoxygenation in a warming world: introduction and overview. *Philosophical Transactions of the Royal Society A*, 375, 20170240. <https://doi.org/10.1098/rsta.2017.0240>
- Siebert, C., McManus, J., Bice, A., Poulson, R., & Berelson, W. M. (2006). Molybdenum isotope signatures in continental margin sediments. *Earth and Planetary Science Letters*, 241, 723–733. <https://doi.org/10.1016/j.epsl.2005.11.010>
- Siebert, C., Nägler, T. F., von Blanckenburg, F., & Kramers, J. D. (2003). Molybdenum isotope records as a potential new proxy for paleo-oceanography. *Earth and Planetary Science Letters*, 211, 159–171. [https://doi.org/10.1016/S0012-821X\(03\)00189-4](https://doi.org/10.1016/S0012-821X(03)00189-4)
- Sinninghe Damsté, J. S., & Köster, J. (1998). A euxinic southern North Atlantic Ocean during the Cenomanian/Turonian oceanic anoxic event. *Earth and Planetary Science Letters*, 158, 165–173. [https://doi.org/10.1016/S0012-821X\(98\)00052-1](https://doi.org/10.1016/S0012-821X(98)00052-1)
- Sullivan, D. L., Brandon, A. D., Eldrett, J., Bergman, S. C., Wright, S., & Minisini, D. (2020). High resolution osmium data record three distinct pulses of magmatic activity during Cretaceous Oceanic Anoxic Event 2 (OAE-2). *Geochimica et Cosmochimica Acta*, 285, 257–273. <https://doi.org/10.1016/j.gca.2020.04.002>
- Sun, X., Zhang, T., Milliken, K. L., & Sun, D. (2016). Geochemical evidence for organic matter source input and depositional environments in the lower and upper Eagle Ford Formation, south Texas. *Organic Geochemistry*, 98, 66–81. <https://doi.org/10.1016/j.orggeochem.2016.05.018>
- Sweere, T. C., Dickson, A. J., Jenkyns, H. C., Porcelli, D., Elrick, M., van den Boorn, S. H. J. M., & Henderson, G. M. (2018). Isotopic evidence for changes in the zinc cycle during Oceanic Anoxic Event 2 (Late Cretaceous). *Geology*, 46, 463–466. <https://doi.org/10.1130/G40226.1>
- Sweere, T. C., Dickson, A. J., Jenkyns, H. C., Porcelli, D., Ruhl, M., Murphy, M. J., et al. (2020). Controls on the Cd-isotope composition of Upper Cretaceous (Cenomanian–Turonian) organic-rich mudrocks from South Texas (Eagle Ford Group). *Geochimica et Cosmochimica Acta*, 287, 251–262. <https://doi.org/10.1016/j.gca.2020.02.019>
- Takashima, R., Nishi, H., Yamanaka, T., Tomosugi, T., Fernando, A. G., Tanabe, K., et al. (2011). Prevailing oxic environments in the Pacific Ocean during the mid-Cretaceous Oceanic Anoxic Event 2. *Nature Communications*, 2, 2234. <https://doi.org/10.1038/ncomms1233>
- Turgeon, S. C., & Creaser, R. A. (2008). Cretaceous Oceanic Anoxic Event 2 triggered by a massive magmatic episode. *Nature*, 474, 323–326. <https://doi.org/10.1038/nature07076>
- Vorlicek, T., Helz, G. R., Chappaz, A., Vue, P., Vezina, A., & Hunter, W. (2019). Molybdenum burial mechanism in sulfidic sediments: Iron-sulfide pathway. *ACS Earth and Space Chemistry*, 2, 565–576. <https://doi.org/10.1021/acsearthspacechem.8b00016>
- Watson, A. J., Lenton, T. M., & Mills, B. J. W. (2017). Ocean deoxygenation, the global phosphorus cycle and the possibility of human-caused large-scale ocean anoxia. *Philosophical Transactions of the Royal Society A*, 375, 20160318. <https://doi.org/10.1098/rsta.2016.0318>
- Weiss, R. F. (1970). The solubility of nitrogen, oxygen and argon in water and seawater. *Deep-Sea Research and Oceanographic Abstracts*, 17, 721–735. [https://doi.org/10.1016/0011-7471\(70\)90037-9](https://doi.org/10.1016/0011-7471(70)90037-9)
- Westermann, S., Vance, D., Cameron, V., Archer, C., & Robinson, S. A. (2014). Heterogeneous oxygenation states in the Atlantic and Tethys oceans during Oceanic Anoxic Event 2. *Earth and Planetary Science Letters*, 404, 178–189. <https://doi.org/10.1016/j.epsl.2014.07.018>
- Wiedmann, J., Butt, A., & Einsele, G. (1978). Vergleich von marokkanischen Kreide-Küstenaufschlüssen und Tiefseebohrungen (DSDP): Stratigraphie, Paläoenvironment und Subsidenz an einem passiven Kontinentalrand. *Geologische Rundschau*, 67, 454508. <https://doi.org/10.1007/BF01802800>
- Wohlwend, S., Hart, M., & Weissert, H. (2015). Ocean current intensification during the Cretaceous oceanic anoxic event 2: Evidence from the northern Tethys. *Terra Nova*, 27, 147–155. <https://doi.org/10.1111/ter.12142>